

ANALYTICAL GUIDANCE FOR SPACECRAFT RELATIVE MOTION UNDER CONSTANT THRUST USING RELATIVE ORBIT ELEMENTS

Riccardo Bevilacqua,^{*} and Thomas Alan Lovell[†]

This paper introduces novel analytical guidance solutions for spacecraft relative motion considering continuous, on-off thrust, and using Relative Orbit Elements as a geometrical representation of the dynamics. The solutions provide the relative state vector at any given time, accommodating any thrust magnitude along the three directions of the relative frame, as well as generic activation times and durations. Relative Orbit Elements geometrically interpret key aspects of the relative motion, including for example, the relative ellipse size, and the evolution of its center in time. The new solutions provide the guidance designer with a direct visualization of the thrust effects on the relative motion geometry, offering new possibilities for analytical guidance in the presence of continuous thrust engines, such as low thrust engines on nano-spacecraft. The paper presents the analytical solutions, and tests their effectiveness using a sample guidance thrust profile based on input-shaping, previously developed by one of the authors using classical Cartesian coordinates. The use of Relative Orbit Elements shows substantial benefits and added simplicity with respect to Cartesian-based approaches.

INTRODUCTION

Spacecraft relative motion is commonly represented in a relative frame using Cartesian coordinates. Relative Orbit Elements (ROEs) represent a nonlinear transformation from Cartesian coordinates to geometric variables, giving a visual and straightforward understanding of the main aspects of proximity flight dynamics. This paper presents the general analytical solution for the time evolution of the ROEs, when on/off constant thrust is used. These results are of particular interest for missions employing low thrust engines. The new solutions hold the potential for on-board implementation. Alternately, given their analytical nature, they may serve as an initial guess for numerical optimizers to minimize fuel/time, and enable verification of various pre-designed thrust profiles. In this paper the authors demonstrate the last feature, by deriving solutions for orbital re-phasing (moving to a new location along track) or rendezvous (moving to the location of a chief satellite, i.e. the origin of the relative motion frame) using thrust profiles based on input shaping.

^{*} Assistant Professor, Mechanical, Aerospace, and Nuclear Engineering Department, Rensselaer Polytechnic Institute, 110 8th street, Troy, NY, 12180, USA. bevilr@rpi.edu

[†] Research Aerospace Engineer, Air Force Research Laboratory, Space Vehicles Directorate, Kirtland AFB, NM.

Input shaping has been extensively used in vibration suppression for flexible manipulators (References 1-8), but never for orbital control, to the authors' knowledge. Input shaping is a convolution technique based on the knowledge of a system's natural frequencies of oscillation. Given a feed-forward control signal, designed to perform a desired maneuver, but not taking into account potential excitation of undesired oscillations, input shaping consists of the convolution of the signal itself and a specified train of impulses, so that the system's resulting behavior presents minimal residual vibrations at the end of the maneuver. The impulses and their locations in time are computed based on the frequencies that need to be suppressed, i.e. the modes one wants to limit in amplitude. The majority of input shaping applications falls under the category of flexible structures control, such as space manipulators control. It is important to underline that input shaping is not intended to reduce the energy of a system. Roughly speaking, existing oscillations cannot be damped with input shaping, while maneuvers from a stable set to a new stable set are possible, as in the case of re-phasing maneuvers. In the specific context of spacecraft relative motion, oscillations refer to periodic motion in the position coordinates.

Exploiting the new analytical formulas, the special case of an input shaping profile is presented, and the analytical solution for spacecraft rendezvous with along-track control only is derived. In addition, the paper demonstrates how the input shaped control profile can be ad-hoc modified to obtain a final close relative motion of desired size relative to a reference satellite. Sample numerical simulations show some of the maneuvers achieved via the analytical solutions.

SATELLITE RELATIVE DYNAMICS

Consider two satellites orbiting in close proximity to each other. For this analysis, one will be referred to as the reference satellite, or "chief," and the other as the "deputy." For the methods presented here, it is assumed that the only force acting on each satellite is that of a point mass gravitational field, the chief is in a circular orbit, and the distance between the satellites is small compared to their orbital radius. These assumptions yield the following linear time-invariant differential equations:⁹⁻¹⁰

$$\begin{aligned} \ddot{x} - 2n \dot{y} - 3n^2 x &= 0 \\ \ddot{y} + 2n \dot{x} &= 0 \\ \ddot{z} + n^2 z &= 0 \end{aligned} \tag{1}$$

These are known as the Hill's-Clohessy-Wiltshire (HCW) equations and are written in the local-vertical, local-horizontal (LVLH) coordinate frame, whose origin is at the chief satellite. In these equations, x is the component of the deputy's position vector relative to the chief in the radial direction positive away from the Earth, y is the along-track component positive along the velocity vector of the chief, and z is the cross-track component perpendicular to the orbital plane of the chief. n is the mean motion of the chief. The LVLH frame is depicted in Figure 1.

The solution to Equations (1) is:

$$\begin{aligned}
x &= \frac{\dot{x}_0}{n} \sin(nt) - (3x_0 + \frac{2\dot{y}_0}{n}) \cos(nt) + (4x_0 + \frac{2\dot{y}_0}{n}) \\
y &= \frac{2\dot{x}_0}{n} \cos(nt) + (6x_0 + \frac{4\dot{y}_0}{n}) \sin(nt) - (6nx_0 + 3\dot{y}_0)t - \frac{2\dot{x}_0}{n} + y_0 \\
z &= \frac{\dot{z}_0}{n} \sin(nt) + z_0 \cos(nt) \\
\dot{x} &= \dot{x}_0 \cos(nt) + (3nx_0 + 2\dot{y}_0) \sin(nt) \\
\dot{y} &= -2\dot{x}_0 \sin(nt) + (6nx_0 + 4\dot{y}_0) \cos(nt) - (6nx_0 + 3\dot{y}_0) \\
\dot{z} &= \dot{z}_0 \cos(nt) - nz_0 \sin(nt)
\end{aligned} \tag{2}$$

where x_0, y_0 , etc, are conditions at some epoch time t_0 , and t is the time since t_0 . Consider the following change of coordinates from $x, y, z, \dot{x}, \dot{y}, \dot{z}$:¹¹

$$\begin{aligned}
a_e &= 2\sqrt{\left(\frac{\dot{x}}{n}\right)^2 + \left(3x + 2\frac{\dot{y}}{n}\right)^2} & x_d &= 4x + 2\frac{\dot{y}}{n} \\
y_d &= y - 2\frac{\dot{x}}{n} & \beta &= \text{atan2}(\dot{x}, 3nx + 2\dot{y}) \\
z_{\max} &= \sqrt{\left(\frac{\dot{z}}{n}\right)^2 + z^2} & \gamma &= \text{atan}(nz, \dot{z}) - \text{atan2}(\dot{x}, 3nx + 2\dot{y})
\end{aligned} \tag{3}$$

where $a_e, x_d, y_d, \beta, z_{\max}$ and γ are the ROEs. The inverse of this transformation is

$$\begin{aligned}
x &= \frac{-a_e}{2} \cos \beta + x_d & \dot{x} &= \frac{a_e}{2} n \sin \beta \\
y &= a_e \sin \beta + y_d & \dot{y} &= a_e n \cos \beta - \frac{3}{2} nx_d \\
z &= z_{\max} \sin(\gamma + \beta) & \dot{z} &= z_{\max} n \cos(\gamma + \beta)
\end{aligned} \tag{4}$$

It has been shown in Ref. 11 how the ROEs evolve with time:

$$\begin{aligned}
a_e &= a_{e0} & x_d &= x_{d0} \\
y_d &= y_{d0} - \frac{3}{2} nx_{d0}t = y_{d0} - \frac{3}{2} nx_d t & \beta &= \beta_0 + nt \\
z_{\max} &= z_{\max 0} & \gamma &= \gamma_0
\end{aligned} \tag{5}$$

These equations are analogous to Equations (2) for $x, y, z, \dot{x}, \dot{y}, \dot{z}$ in that they express the ROE values at any given time as a function of their initial (epoch) values and the time since epoch.

The parameterization of Equations (4) reveals that the relative motion in the x-y plane of the deputy with respect to the chief is a superposition of periodic motion in x and y, with period equal to that of the chief's orbit, and secular motion in y. Essentially, this is an elliptical path that is drifting in the y-direction at a rate of $-\frac{3}{2}nx_d$. The instantaneous center of the ellipse is (x_d, y_d) .

It has a semi-major axis of length a_e in the along-track direction and semi-minor axis of length $a_e/2$ in the radial direction. β is a parametric angle (i.e. phase angle) indicating the location of the deputy satellite in its trajectory, with $\beta = 0$ corresponding to the perigee location (the "bottom" of the ellipse). The relative motion in x and y, if the elliptical path were "frozen" at a point in time, is depicted in Figure 2. Although the ellipse is actually drifting, it has been frozen in order to conveniently label the ROEs. The z-component of the relative motion, according to the HCW model, is purely sinusoidal and independent of x and y. This motion is a simple harmonic oscillator with amplitude z_{max} and phase angle $\gamma + \beta$. The deputy intersects the chief's orbit plane at $\gamma + \beta = 0$ and π , and reaches z_{max} and $-z_{max}$ at $\gamma + \beta = \pi/2$ and $3\pi/2$, respectively. Thus, γ represents the phase difference between the x-y motion and the z motion. Figure 3 depicts a typical 3-D relative trajectory, with z_{max} and γ labeled. (NOTE: Because β and γ are angular representations of time—similar to mean anomaly—they are labeled in Figures 2 and 3 as β^* and γ^* , which are the physical interpretations of these angles.)

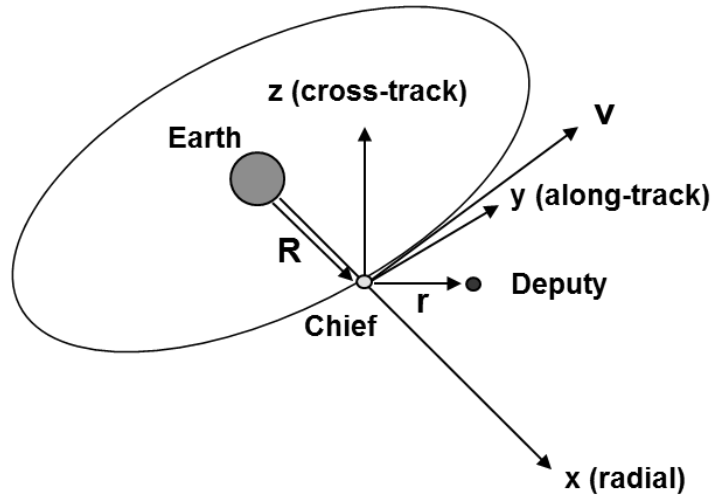


Figure 1. Depiction of LVLH Frame.

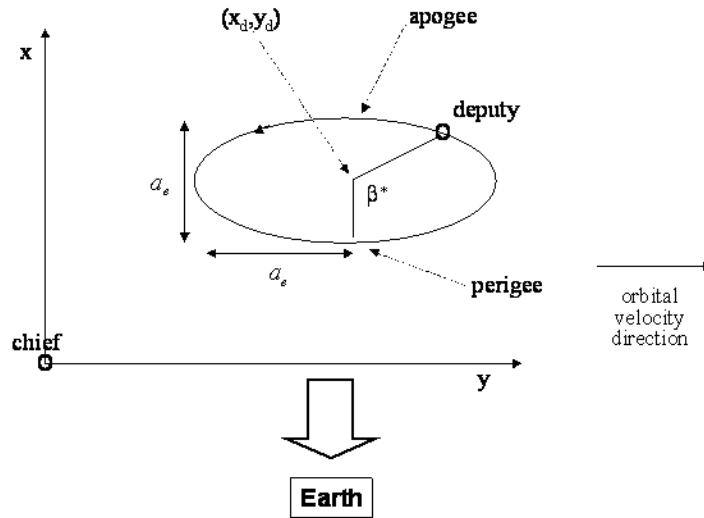


Figure 2. Planar Projection of Relative Motion Trajectory with Relative Orbit Elements Labeled.

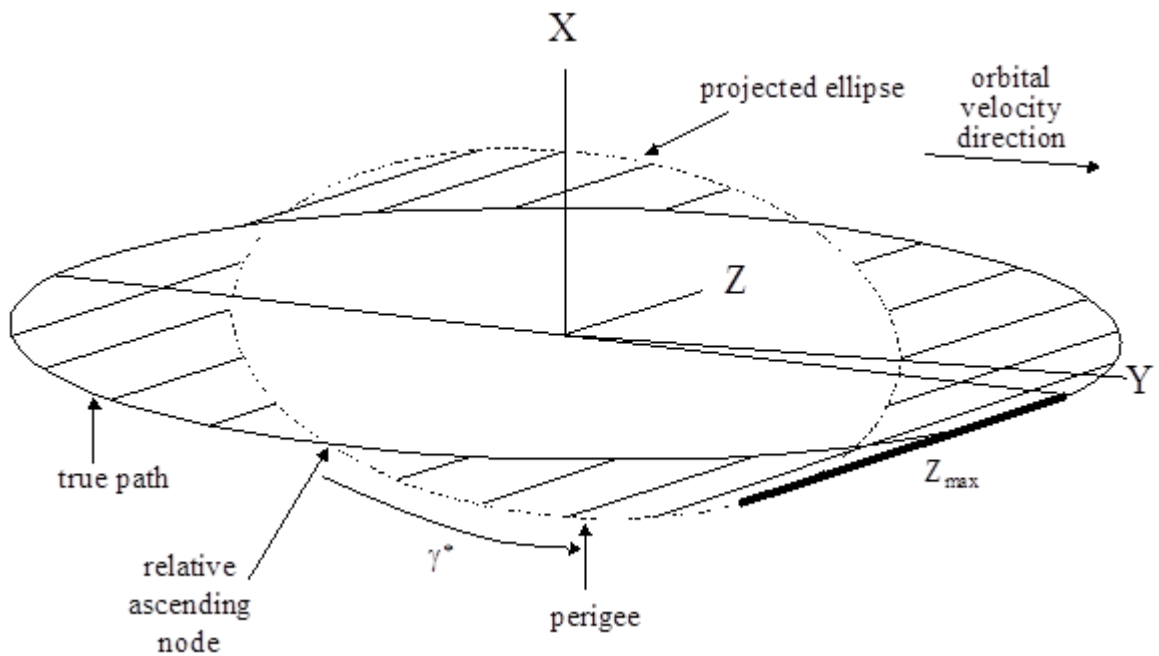


Figure 3. Depiction of Out-of-Plane Relative Motion with Relative Orbit Elements Labeled.

ANALYTICAL SOLUTIONS WITH CONTINUOUS ON-OFF THRUST

This section presents the steps to derive the closed-form solutions for the time evolution of the ROEs when a generic on-off, continuous thrust profile is assumed in each direction of the LVLH reference frame. $A_{x,y,z,i}$ indicates the magnitude of the i -th firing in the x , y , or z direction. $\Delta t_{x,y,z,i}$ is

the corresponding time duration of the firing, while $t_{f_{x,y,z,i}}$ is the coasting (off) time duration between the $(i-1)$ -th and the i -th firing. t_F is the final time (see Figure 4). Note that, if the first firing in a particular direction begins at $t = 0$, then t_{f_i} in that direction is defined to be 0.

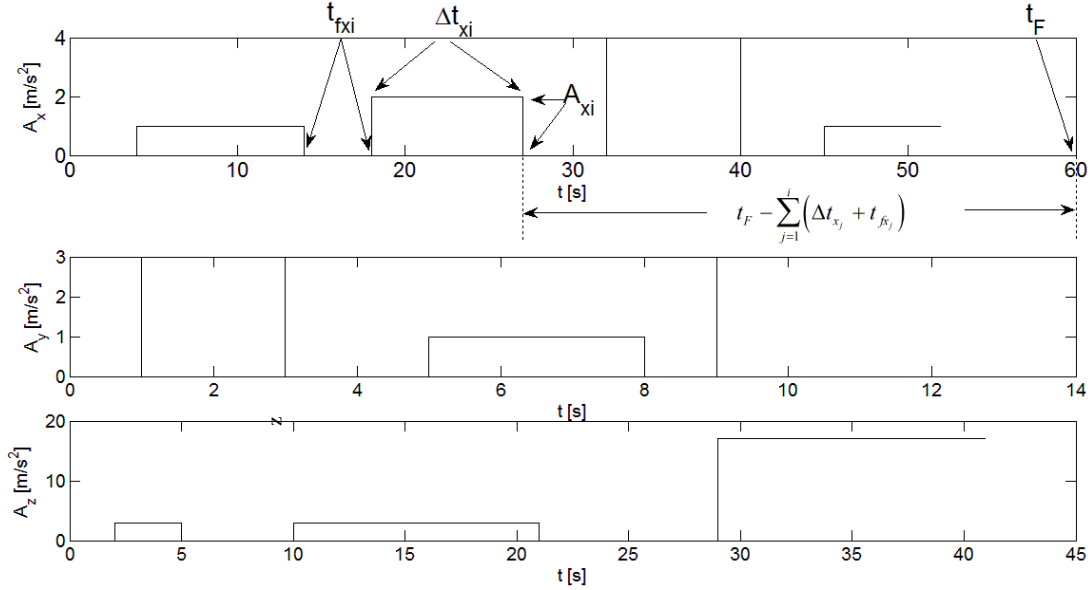


Figure 4. Generic example of on-off continuous thrust profile.

Because the dynamics are linear, the superposition principle can be applied to find the state at the final time. In particular, the final state can be written as the sum of the value at the final time when coasting from the initial condition, plus each of the final values obtained by starting at zero

initial conditions, coasting for a duration equal to $\sum_1^{i-1} (t_{f_j} + \Delta t_j) + t_{f_i}$, applying the generic i -th

thrust for its given duration, and then coasting for a duration equal to $t_F - \sum_{j=1}^i (\Delta t_j + t_{f_j})$. In the

previous expressions the subscript indicating the direction of the firing was removed, indicating its validity for any axis. For each of the x, y, and z components, the ROEs offer a simple solution, since coasting from a set of initial conditions is represented by the equations:

$$\begin{aligned}
 a_e &= a_{e0} \\
 x_d &= x_{d0} \\
 y_d &= y_{d0} - \frac{3}{2} n x_{d0} t_F \\
 \beta &= \beta_0 + n t_F \\
 z_{\max} &= z_{\max 0} \\
 \gamma &= \gamma_0
 \end{aligned} \tag{6}$$

Finding the final state after firing from zero initial conditions, and then coasting, requires the combination of Cartesian coordinates to find the state right after firing, then conversion to ROEs, and finally coasting, using the same form as in Equation (6). The following equations give the values of the Cartesian relative states after a generic single firing of duration Δt and coasting pe-

riod t beforehand, with components in the x, y, and z directions. They can be easily derived using Laplace transform on the system in Equations (1):

$$\begin{aligned}
x^+ &= \frac{A_x}{n^2} [1 - \cos(n\Delta t)] + 2 \frac{A_y}{n} \left[t - \frac{\sin(n\Delta t)}{n} \right] \\
y^+ &= 4 \frac{A_y}{n^2} [1 - \cos(n\Delta t)] - 2 \frac{A_x}{n} \left[t - \frac{\sin(n\Delta t)}{n} \right] - \frac{3}{2} A_y t^2 \\
z^+ &= \frac{A_z}{n^2} [1 - \cos(n\Delta t)] \\
\dot{x}^+ &= \frac{A_x}{n} \sin(n\Delta t) + 2 \frac{A_y}{n} [1 - \cos(n\Delta t)] \\
\dot{y}^+ &= 4 \frac{A_y}{n} \sin(n\Delta t) - 2 \frac{A_x}{n} [1 - \cos(n\Delta t)] - 3 A_y \Delta t \\
\dot{z}^+ &= \frac{A_z}{n} \sin(n\Delta t)
\end{aligned} \tag{7}$$

Equation 3 is then used to convert the Cartesian relative states into ROEs, and the ROEs are propagated for the coasting period according to Equation (6). This is repeated for each single firing, with N_x , N_y , N_z indicating the total number of firings along each axis. By adding together all the states obtained as described above, the following closed-form solutions for the ROEs subject to generic thrust profiles are obtained:

$$a_e(t_F) = 2 \left(\begin{array}{l} \left(\begin{array}{l} (a_{e_0}/2) \sin(\beta_0 + nt_F) \\ - \sum_{i=1}^{N_x} \sqrt{-(2/n^4) A_{x_i}^2 (-1 + \cos(n\Delta t_{x_i}))} \sin \left(-\beta_{x_i}^+ - n \left(t_F - \sum_{j=1}^i (\Delta t_{x_j} + t_{fx_j}) \right) \right) \\ + 2 \sum_{i=1}^{N_y} \sqrt{-(2/n^4) A_{y_i}^2 (-1 + \cos(n\Delta t_{y_i}))} \sin \left(\beta_{y_i}^+ + n \left(t_F - \sum_{j=1}^i (\Delta t_{y_j} + t_{fy_j}) \right) \right) \end{array} \right)^2 \\ + \\ \left(\begin{array}{l} (a_{e_0}/2) \cos(\beta_0 + nt_F) \\ - \sum_{i=1}^{N_x} \sqrt{-(2/n^4) A_{x_i}^2 (-1 + \cos(n\Delta t_{x_i}))} \cos \left(-\beta_{x_i}^+ - n \left(t_F - \sum_{j=1}^i (\Delta t_{x_j} + t_{fx_j}) \right) \right) \\ + 2 \sum_{i=1}^{N_y} \sqrt{-(2/n^4) A_{y_i}^2 (-1 + \cos(n\Delta t_{y_i}))} \cos \left(\beta_{y_i}^+ + n \left(t_F - \sum_{j=1}^i (\Delta t_{y_j} + t_{fy_j}) \right) \right) \end{array} \right)^2 \end{array} \right) \quad (8a)$$

$$\beta_{x_i}^+ = a \tan 2 \left((A_{x_i}/n) \sin(n\Delta t_{x_i}), -(A_{x_i}/n) (1 - \cos(n\Delta t_{x_i})) \right)$$

$$\beta_{y_i}^+ = a \tan 2 \left((2A_{y_i}/n) (1 - \cos(n\Delta t_{y_i})), (2A_{y_i}/n) \sin(n\Delta t_{y_i}) \right)$$

$$\begin{aligned}
x_d(t_F) &= x_{d_0} + (2/n) \sum_{i=1}^{N_y} A_{y_i} \Delta t_{y_i} \\
y_d(t_F) &= y_{d_0} - (3/2) n x_{d_0} t_F - (2/n) \sum_{i=1}^{N_x} A_{x_i} \Delta t_{x_i} - (3/2) \sum_{i=1}^{N_y} A_{y_i} \Delta t_{y_i}^2 \\
&\quad - 3 \sum_{i=1}^{N_y} A_{y_i} \Delta t_{y_i} \left(t_F - \sum_{j=1}^i (\Delta t_{y_j} + t_{fy_j}) \right)
\end{aligned} \quad (8b)$$

$$\beta(t_F) = a \tan 2 \left(\begin{array}{l} \left(\begin{array}{l} a_{e_0} n^2 \sin(\beta_0 + nt_F) - \\ (1/2n) \sum_{i=1}^{N_x} 2A_{x_i} \sqrt{(2 - 2 \cos(n\Delta t_{x_i}))} \sin \left(-\beta_{x_i}^+ - nt_F + n \sum_{j=1}^i (\Delta t_{x_i} + t_{f_{x_i}}) \right) - \\ \sum_{i=1}^{N_y} 4A_{y_i} \sqrt{(2 - 2 \cos(n\Delta t_{y_i}))} \sin \left(-\beta_{y_i}^+ - nt_F + n \sum_{j=1}^i (\Delta t_{y_i} + t_{f_{y_i}}) \right) \end{array} \right) \\ \left(\begin{array}{l} a_{e_0} n^2 \cos(\beta_0 + nt_F) + \\ (1/2n) \sum_{i=1}^{N_x} 2A_{x_i} \sqrt{(2 - 2 \cos(n\Delta t_{x_i}))} \cos \left(-\beta_{x_i}^+ - nt_F + n \sum_{j=1}^i (\Delta t_{x_i} + t_{f_{x_i}}) \right) + \\ \sum_{i=1}^{N_y} 4A_{y_i} \sqrt{(2 - 2 \cos(n\Delta t_{y_i}))} \cos \left(-\beta_{y_i}^+ - nt_F + n \sum_{j=1}^i (\Delta t_{y_i} + t_{f_{y_i}}) \right) \end{array} \right) \end{array} \right)$$

$$\beta_{x_i}^+ = a \tan 2 \left(\left(A_{x_i} / n \right) \sin \left(n\Delta t_{x_i} \right), - \left(A_{x_i} / n \right) \left(1 - \cos \left(n\Delta t_{x_i} \right) \right) \right)$$

$$\beta_{y_i}^+ = a \tan 2 \left(\left(2A_{y_i} / n \right) \left(1 - \cos \left(n\Delta t_{y_i} \right) \right), \left(2A_{y_i} / n \right) \sin \left(n\Delta t_{y_i} \right) \right) \tag{8c}$$

$$\begin{aligned}
z_{\max}(t_F) &= \left(\begin{aligned} & z_{\max_0} \cos(\gamma_0 + \beta_0 + nt_F) + \\ & \left(\sum_{i=1}^{N_z} \sqrt{(A_{z_i}/n^2)(2-2\cos(n\Delta t_{z_i}))} \cos\left(-\psi_i - n\left(t_F - \sum_{j=1}^i (\Delta t_{z_i} + t_{f_{z_i}})\right)\right) \right) \end{aligned} \right)^2 + \\
& \left(\begin{aligned} & z_{\max_0} \sin(\gamma_0 + \beta_0 + nt_F) - \\ & \left(\sum_{i=1}^{N_z} \sqrt{(A_{z_i}/n^2)(2-2\cos(n\Delta t_{z_i}))} \sin\left(-\psi_i - n\left(t_F - \sum_{j=1}^i (\Delta t_{z_i} + t_{f_{z_i}})\right)\right) \right) \end{aligned} \right)^2 \\
\psi_i &= a \tan 2\left(\left(A_{z_i}/n\right)\left(1-\cos(n\Delta t_{z_i})\right), \left(A_{z_i}/n\right)\sin(n\Delta t_{z_i})\right) \\
\gamma(t_F) &= a \tan 2 \left(\begin{aligned} & nz_{\max_0} \sin(\gamma_0 + \beta_0 + nt_F) - \\ & \sum_{i=1}^{N_z} \left(A_{z_i}/n\right) \sqrt{2-2\cos(n\Delta t_{z_i})} \sin\left(-\psi_i - n\left(t_F - \sum_{j=1}^i (\Delta t_{z_i} + t_{f_{z_i}})\right)\right), \\ & nz_{\max_0} \cos(\gamma_0 + \beta_0 + nt_F) + \\ & \sum_{i=1}^{N_z} \left(A_{z_i}/n\right) \sqrt{2-2\cos(n\Delta t_{z_i})} \cos\left(-\psi_i - n\left(t_F - \sum_{j=1}^i (\Delta t_{z_i} + t_{f_{z_i}})\right)\right) \end{aligned} \right) \quad (8d) \\
\psi_i &= a \tan 2\left(\left(A_{z_i}/n\right)\left(1-\cos(n\Delta t_{z_i})\right), \left(A_{z_i}/n\right)\sin(n\Delta t_{z_i})\right)
\end{aligned}$$

EXAMPLE OF APPLICATION OF THE ROE FORMULAS: INPUT SHAPING THRUST PROFILE

In this section a validation of the Equations (8) is performed. In particular, one of the results previously obtained by one of the authors using Cartesian coordinates (Reference 12) is confirmed by means of ROEs, obtaining a simpler expression. In Reference 12, an input-shaping-based, y-only thrust profile was devised as an effective means to obtain analytical leader-follower re-phasing or rendezvous guidance, as well as stable-relative-orbit to stable-relative-orbit guidance. Such a profile allows for in-plane control, moving the center of the ellipse to a new desired location, where the ellipse collapses to a point for leader-follower maneuvers. The thrust profile was derived in Reference 12 as follows:

$$\begin{aligned}
A_{x_i} &= A_{z_i} = 0 & u &= c \cdot \text{sign}(y_{d_0} - y_{d_f}), c > 0 & t_F &= 3t^* + 2\Delta t_w \\
A_{1,2,5,6} &= \pm \pm \frac{1}{4}u, & t_{f_{1,2,4,6}} &= 0, & \Delta t_{1,\dots,6} &= \frac{t^*}{2} \\
A_{3,4} &= \pm \frac{1}{2}u, & t_{f_{3,5}} &= \Delta t_w
\end{aligned} \quad (9)$$

The profile of Equation (9) consists of known amplitudes for the firings (c is a given control amplitude), while the Δt_w and t^* are to be determined. Substituting Equation (9) into Equation (8b) and assuming $y_{d0} > y_{df}$, the following expressions are obtained:

$$\begin{aligned}
x_d(t_F) &= x_{d_0} \\
y_d(t_F) &= y_{d_0} - (3/4)c(t^*)^2
\end{aligned} \tag{10}$$

Equation (10) leads to the solution for t^* , given initial and desired final values for y_d , that is, initial and final centers of the ellipse of relative motion.

$$t^* = \sqrt{4 \frac{y_{d_0} - y_d(t_F)}{3u}} \tag{11}$$

Note that this result is not as straightforward to find in Cartesian coordinates (Reference 12), in which case there is no geometrical interpretation.

Substitution of the profile of Equation (9) in Equation (8a) does not lead to an expression of comparable simplicity. Nevertheless, several observations can be made that provide useful insight with regards to the expected final value for a_e . First of all, all the terms where thrust along x appears are zero. Secondly, the terms not containing a_{e0} in Equation (8a), in the square powers, represent modifications with respect to the initial value of a_e . In fact, if no thrusting was present, the final value for a_e would be a_{e0} , as expected. These observations justify focusing on only some of the resulting terms in Equation (8a), and specifically we here analyze the following portion, where the square power is omitted for simplicity:

$$2 \sum_{i=1}^{N_y} \sqrt{-(2/n^4) A_{y_i}^2 (-1 + \cos(n\Delta t_{y_i}))} \sin \left(\beta_{y_i}^+ + n \left(t_F - \sum_{j=1}^i (\Delta t_{y_j} + t_{f_j}) \right) \right) \tag{12}$$

After some algebra, and the use of Prosthaphaeresis formulas, Equation (12) becomes:

$$\frac{1}{2} \sqrt{\frac{2u^2}{n^4} \left(1 - \cos \left(n \frac{t^*}{2} \right) \right)} \left(\begin{aligned} &2 \sin \left(\beta_y^+ + nt^* + n\Delta t_w \right) \cos \left(nt^* + n\Delta t_w \right) + \\ &+ 2 \sin \left(\beta_y^+ + n \frac{5}{4} t^* + n\Delta t_w \right) \cos \left(nt^* + n\Delta t_w \right) + \\ &+ 4 \sin \left(\beta_y^+ + n \frac{5}{4} t^* + n\Delta t_w \right) \cos \left(n \frac{t^*}{2} \right) \end{aligned} \right) \tag{13}$$

where the $\beta_{y_i}^+$ become a common β_y^+ , given the nature of the firings of same duration in the profile of Equation (9). Equation (13) still provides little information about what to expect at the end of the firing sequence. Since t^* is determined in Equation (11), as well as the β_y^+ , through Equations (8), the only free variable in Equation (13) is the wait time between the series of firings Δt_w . One observation to be made is that the term under the square root is never expected to be zero, since it would imply firing with no duration. For this reason we need only focus on the parenthesis term. The derivative of this parenthesis term with respect to Δt_w yields

$$\begin{aligned}
& 2 \cos\left(\beta_y^+ + n\Delta t_w + \frac{3}{4}nt^*\right) + 2 \cos\left(\beta_y^+ + n\Delta t_w + \frac{7}{4}nt^*\right) + \\
& + 2 \cos\left(\beta_y^+ + 2n\Delta t_w + 2nt^*\right) + 2 \cos\left(\beta_y^+ + 2n\Delta t_w + \frac{9}{4}nt^*\right)
\end{aligned} \tag{14}$$

This shows that at the most four values for Δt_w can represent a minimum/maximum for Equation (13), within an orbital period ($0 \leq \Delta t_w \leq T$). In fact, such a derivative is composed of four cosine functions, all shifted by different phases.

The location of these minimum/maximum points changes from case to case, depending on the β_y^+ and t^* . Despite the impracticability of solving Equation (8a) in terms of Δt_w , even when simplified with the input shaping profile, the derivative information allows us to predict the type of function we should expect, and, in addition, Equation (13) clearly shows a content in frequency, when using Δt_w as independent variable, not exceeding $2n$. The Nyquist–Shannon sampling theorem (Reference 13) enables capturing the nature of the function representing a_e when input shaping is applied, and Δt_w is the independent variable, by computing Eq. (8a) only at Δt points spaced by a $1/4n$ distance, that is, theoretically 8π (i.e. 25 or more) points total in one orbital period time frame. A desired a_e value can be then interpolated using these required values (e.g. using splines), or more points, for increased accuracy purposes, posing no computational issues.

Depending on the initial conditions, the extrema can be four or less, and located at different Δt_w values between 0 and the orbital period T , as shown later on. In all cases there are special values of Δt_w that zero out the increase in a_e , that is, there are no oscillation size increases due to performing the maneuver.

It should be noted that for the other term under the radical in Equation (8a), an identical expression can be found, the only difference being that the sine function in Equation (12) would be replaced by a cosine function. Thus, the analysis of this term would be quite similar to that above.

SAMPLE NUMERICAL SIMULATIONS

In the following numerical simulations we assume a chief satellite located at the origin of the LVLH frame, and that we are maneuvering a deputy satellite. The chief represents the target trajectory for the different types of maneuvers here presented, i.e. we set up rendezvous problems. More generally, such a target trajectory can be a virtual satellite, and can be located anywhere such that the chief and deputy orbital periods are equal. The following numerical simulations are obtained using the results presented earlier. For all the simulations the control value $c=2 \cdot 10^{-5}$ m/s² is used, typical of atmospheric differential drag control in low Earth orbits.¹⁴ In principle, any c value can be chosen, representing the thrust available on the spacecraft. The initial orbital parameters of Table 1 are used to generate the trajectories for the first simulation, representing an initial condition of leader-follower. Note that the initial orbital parameters are first converted to Cartesian position and velocity in an Earth centered inertial frame, then translated kinematically into the LVLH frame, and finally forced to match a leader follower initial condition for the linear equations, i.e., cancelling any residual relative velocity and x displacement. Three different final conditions are chosen for this simulation, one being exact rendezvous and two cases where the final motion is a relative closed orbit around the chief. For these cases, the variation of final a_e as function of Δt_w reduces to a simple cosine function, with maximum at 0 and one orbital period,

and no increase at one-half orbital period (see Figure 5). Figure 6 shows the resulting trajectories applying input shaping, as well as the control profiles as dictated by Equation (9).

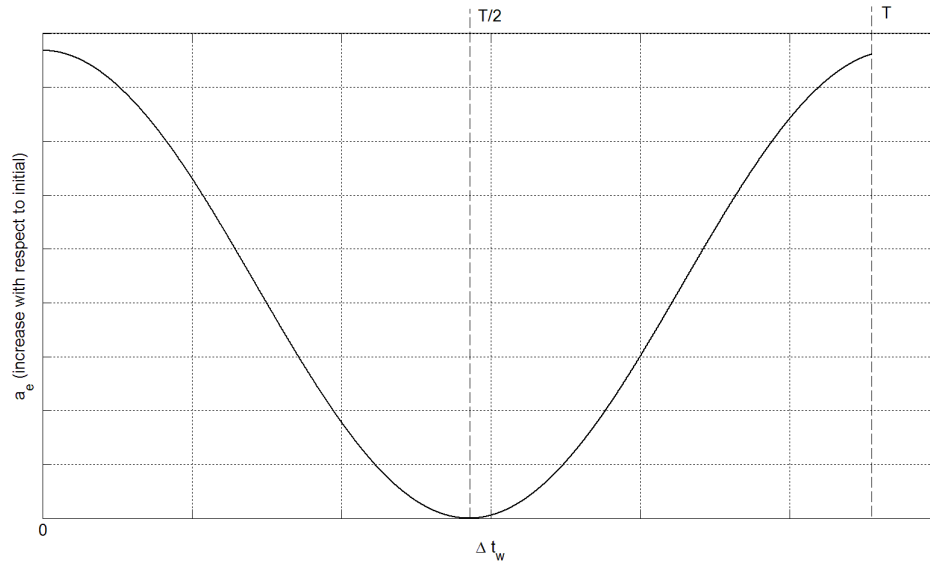


Figure 5 Example of a_e vs. Δt_w for leader follower initial condition. Note: the above graph is obtained using the numerical data of Table 1, showing the min and max points.

Table 1: Initial Orbital parameters for S/C and desired trajectory for Leader-Follower case, plus general data for simulations.

Initial Orbital Parameter	Chief	Deputy
Semi-major axis a	6,778.1 km	6,778.1 km
Eccentricity e	0	0
Inclination i	97.9908 deg	97.9908 deg
Right Ascension of the Ascending Node (RAAN) Ω	261.621 deg	261.621 deg
Argument of Perigee ω_p	30 deg	30 deg
Polar Angle ν	27.216 deg	27.18 deg
Additional parameters used for the simulations		
$J_2 = 108263 \cdot 10^{-8}$ $R_{Earth} = 6378.1363 \text{ km}$ $\mu = 398600.4418 \text{ km}^3/\text{s}^2$		

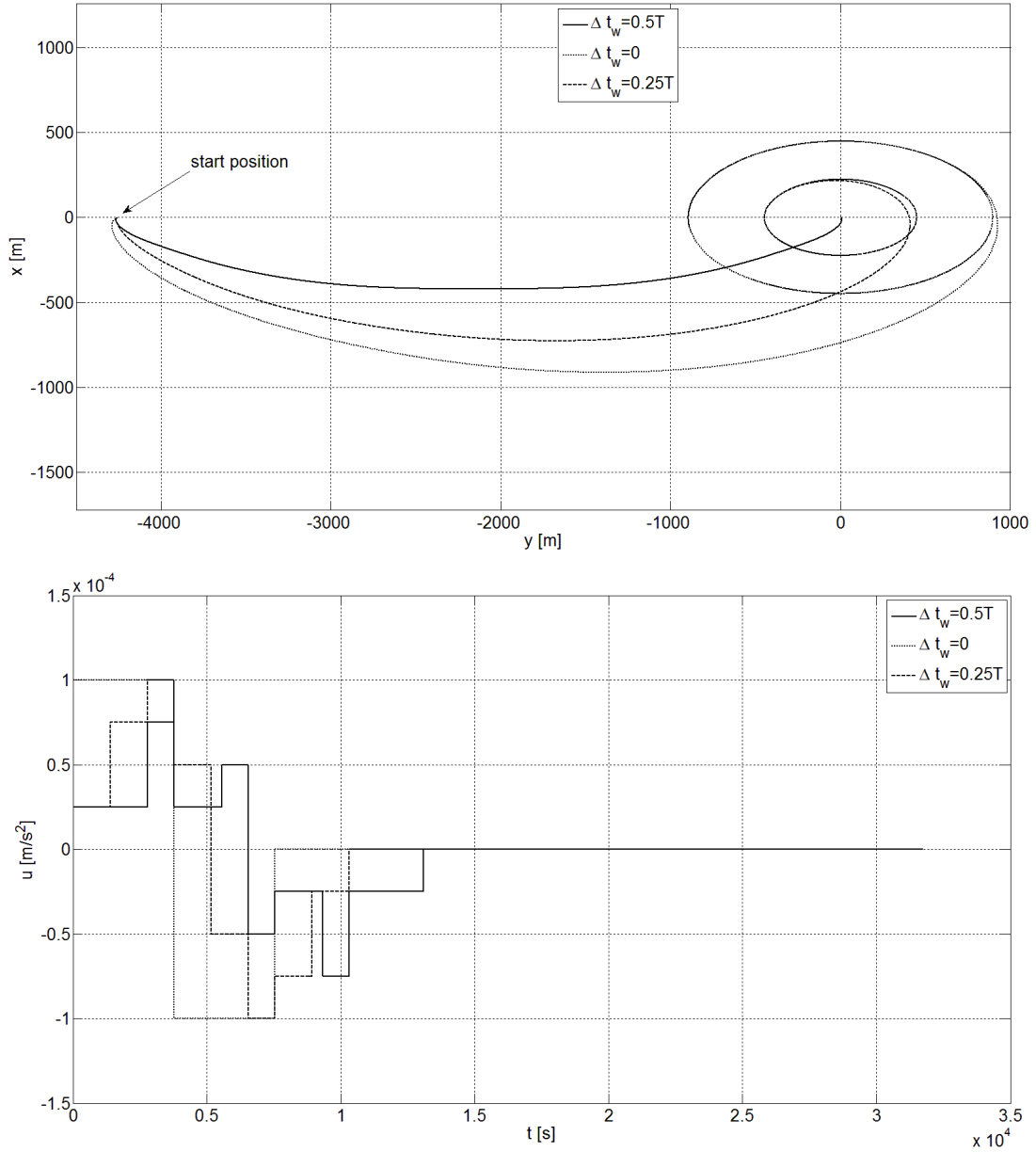


Figure 6 Rendezvous with chief starting from an initial relative point. TOP: 1) $\Delta t_w = 0.5T$, exact rendezvous with chief; 2) $\Delta t_w = 0$, obtaining the maximum a_e for the final stable orbit around the chief; 3) $\Delta t_w = 0.25T$, obtaining an intermediate value of a_e for the final stable relative orbit around the chief. BOTTOM: control profiles.

Table 2 introduces a small eccentricity in the deputy initial orbital parameters, thus creating an initial motion which is a relative closed orbit whose center is offset from the chief by the same amount as the leader-follower separation in the previous cases. Note that the initial orbital parameters are first converted in Cartesian coordinates in an Earth centered inertial frame, then translated kinematically into the LVLH frame, and finally forced to match a stable motion initial condition for the linear equations, i.e., imposing the condition $\dot{y}_0 = -2\omega x_0$.¹⁰ For these scenarios, the final a_e function is more complicated than before. Figure 7 indicates that $\Delta t_w = 625\text{sec}$ yields no change in a_e , $\Delta t_w = 4440\text{sec}$ yields the maximum final value of a_e , and $\Delta t_w = 0.5T$ yields an inter-

mediate final value of a_e . These results are shown in Figure 8, including both the x-y trajectories and the control profiles.

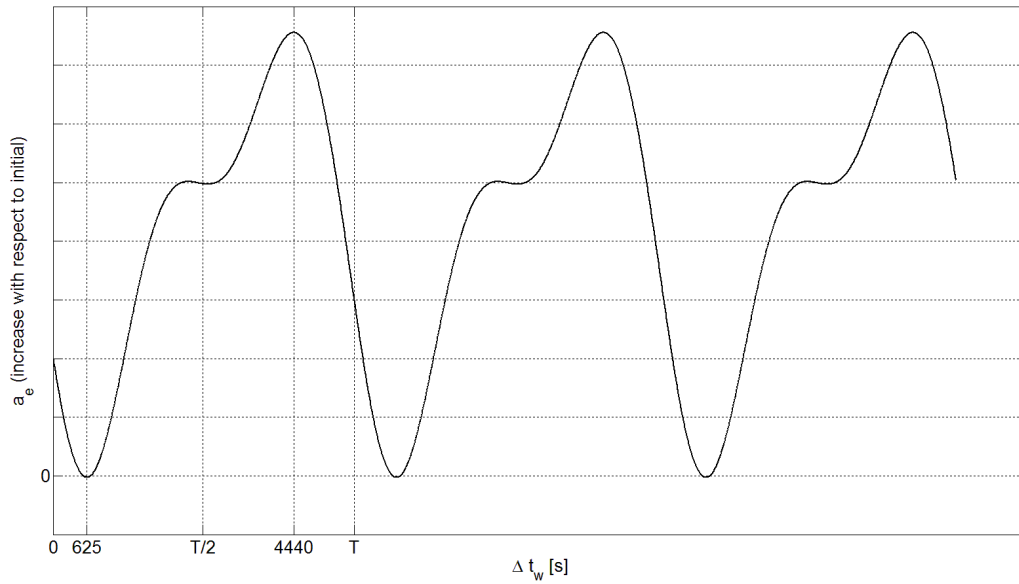


Figure 7 Example of a_e vs. Δt_w for stable relative orbit initial condition. Note: the above graph is obtained using the numerical data of Table 2, showing the min and max points.

Table 2 Initial Orbital parameters for S/C and desired trajectory for Stable-to-Stable case.

Orbital Parameter	Chief	Deputy
Semi-major axis a	6,778.1 km	6,778.1 km
Eccentricity e	0	0.0001
Inclination i	97.9908 deg	97.9908 deg
Right Ascension of the Ascending Node (RAAN) Ω	261.621 deg	261.621 deg
Argument of Perigee ω_p	30 deg	30 deg
Polar Angle ν	27.216 deg	27.18 deg

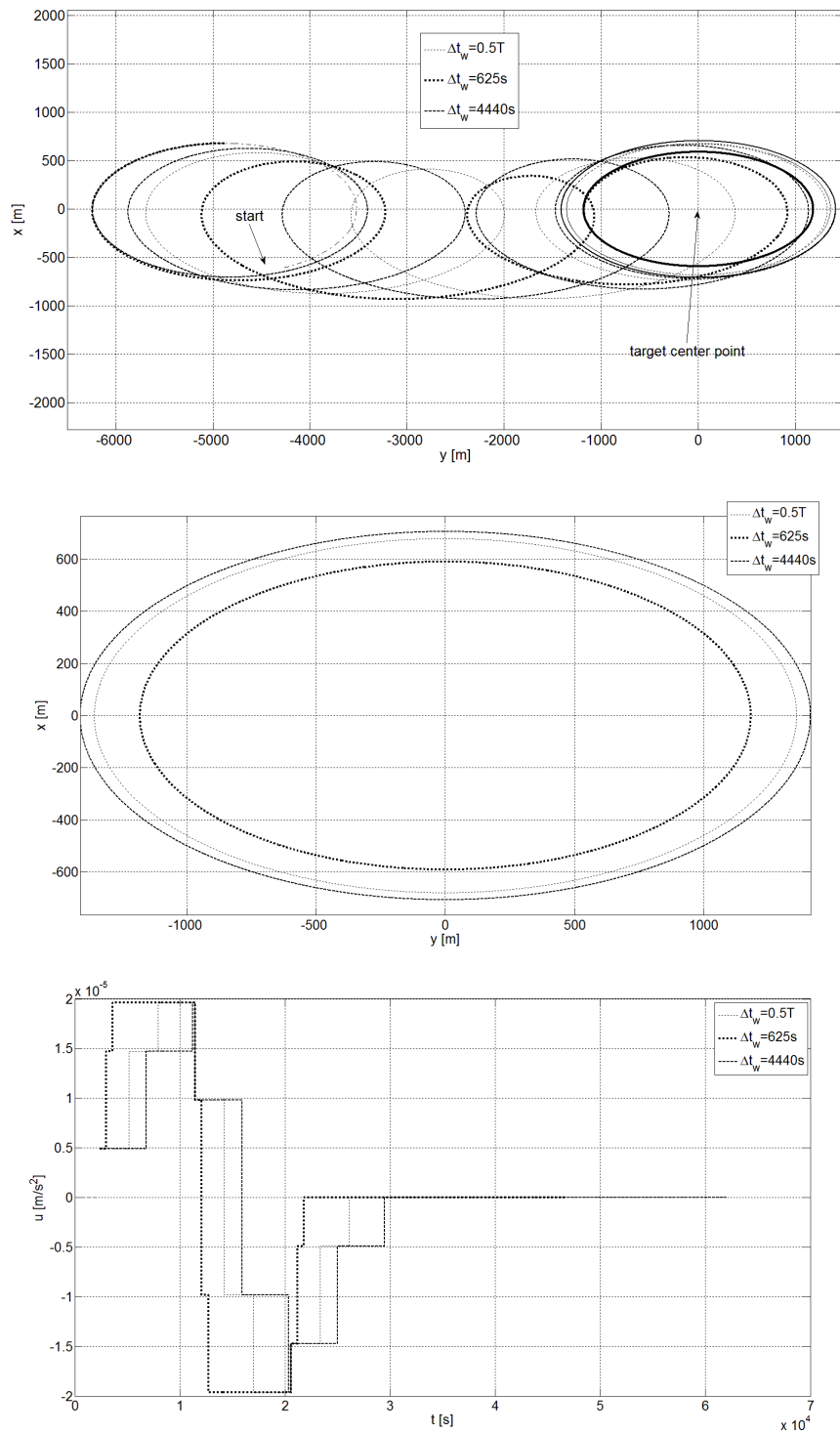


Figure 8 Rendezvous with chief starting from an initial relative stable orbit. TOP: 1) $\Delta t_w = 0.5T$, obtaining an intermediate a_e (between initial and maximum achievable) on final relative orbit; 2) $\Delta t_w = 625s$, obtaining the minimum a_e for the final stable orbit around the chief; 3) $\Delta t_w = 4440s$, obtaining the maximum of a_e for the final stable relative orbit around the chief. CENTER: zoom of the final relative orbits. BOTTOM: control profiles.

All the maneuvers can be computed analytically, from Equation (11) and the earlier observations on the function $a_e(\Delta t_w)$. The only numerical operation required to design such maneuvers consists of reconstructing $a_e(\Delta t_w)$ by means of computing Equation (8a) at a few points, and interpolating when a desired change in a_e is given, to solve for the corresponding Δt_w . This provides a powerful tool to design guidance trajectories onboard spacecraft with limited computing capabilities.

Figure 9 compares three reconstructions of the $a_e(\Delta t_w)$ function: the one using the necessary 8π points, minimally differing from the more accurate line obtained with a sample time of 1 second. The third line shows how less than 8π points (10 in the example) lead to a poor reconstruction of the curve. The circles indicate the $(\Delta t_w, a_e)$ points required for the curve reconstruction. Once those are stored in a table, a desired a_e value leads to the corresponding Δt_w by linearly interpolating between the two closest a_e points.

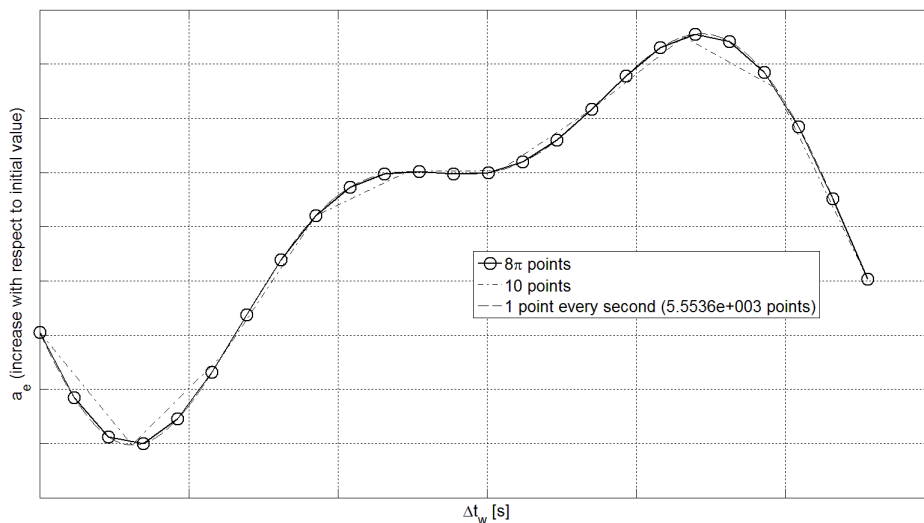


Figure 9 Graphical demonstration of the number of points needed to represent the $a_e(\Delta t_w)$ function.

More generally, the new equations providing the ROEs' time evolution in analytical form, when continuous, on-off thrust is applied, hold the potential for testing and designing new open loop control sequences. They could also provide analytical initial guesses for numerical optimization of the guidance.

CONCLUSION

This paper presents the general analytical solutions for spacecraft relative orbit control, when on/off continuous thrusters are used, employing Relative Orbit Elements instead of classical Cartesian coordinates to represent the relative dynamics. Relative Orbit Elements are a powerful tool to visualize geometrical aspects of spacecraft relative motion. A thrust profile based on the input-shaping technique is used to validate the obtained formulas. The analytical solutions for exact re-phasing or rendezvous using input shaping are provided, along with the expressions and procedures to control the size of the final relative orbit around the target trajectory or chief satellite. Sample numerical simulations show the type of maneuvers achievable using the ROE formulas and input shaping control profiles, namely, re-phasing or rendezvous maneuvers with along-track control only.

ACKNOWLEDGMENTS

The first author wishes to acknowledge the American Society for Engineering Education (ASEE) and the Air Force Research Laboratory, Space Vehicles Directorate, Kirtland AFB, NM, for the opportunity to participate in the 2012 Air Force Summer Faculty Fellowship Program. The results presented were obtained during summer 2012 at AFRL.

REFERENCES

- ¹ A. Banerjee, N. Pedreiro, and W. Singhose, "Vibration Reduction for Flexible Spacecraft Following Momentum Dumping with/without Slewing," *AIAA J. of Guidance, Control, and Dynamics*, vol. 24, pp. 417-428, 2001.
- ² Craig F. Cutforth, Lucy Y. Pao, "Adaptive input shaping for maneuvering flexible structures", *Automatica*, 40 (2004), 685 – 693. doi:10.1016/j.automatica.2003.11.013
- ³ Lucy Y. Pao, "Analysis of the Frequency, Damping, and Total Insensitivities of Input Shaping Designs", *AIAA Journal of Guidance, Control, and Dynamics*, vol. 20, no. 5, 1997.
- ⁴ Matthew D. Baumgart, Lucy Y. Pao, "Discrete time-optimal command shaping", *Automatica* 43 (2007) 1403 – 1409. doi:10.1016/j.automatica.2007.01.003
- ⁵ Mark A. Lau, Lucy Y. Pao, "Input shaping and time-optimal control of flexible structures", *Automatica* 39 (2003) 893 – 900. doi:10.1016/S0005-1098(03)00024-4
- ⁶ Lucy Y. Pao, Craig F. Cutforth, "On Frequency-Domain and Time-Domain Input Shaping for Multi-Mode Flexible Structures", *Journal of Dynamic Systems, Measurement, and Control*, SEPTEMBER 2003, Vol. 125, 494-497. DOI: 10.1115/1.1591808
- ⁷ Lucy Y. Pao, and Mark A. Lau, "Expected Residual Vibration of Traditional and Hybrid Input Shaping Designs", *AIAA Journal of Guidance, Control, and Dynamics*, Vol. 22, no. 1, 1998, 162-165.
- ⁸ M. Romano, B.N. Agrawal, F. Bernelli-Zazzera, "Experiments on Command Shaping Control of a Manipulator with Flexible Links", *AIAA Journal of Guidance, Control, and Dynamics*, Vol. 25, No. 2, 2002, pp. 232-239.
- ⁹ G. W. Hill, "Researches in the Lunar Theory," *American Journal of Mathematics*, Volume 1, 1878, pp. 5-26.
- ¹⁰ W. H. Clohessy and R. S. Wiltshire, "Terminal Guidance System for Satellite Rendezvous", *Journal of the Aerospace Sciences*, Vol. 27, No. 9, 1960, pp. 653-658.
- ¹¹ T. Alan Lovell, Steven G. Tragesser, "GUIDANCE FOR RELATIVE MOTION OF LOW EARTH ORBIT SPACECRAFT BASED ON RELATIVE ORBIT ELEMENTS", *AIAA Paper 2004-4988*, *AIAA/AAS Astrodynamics Specialist Conference and Exhibit*, Providence, Rhode Island, 2004/08/16 - 2004/08/19.
- ¹² Riccardo Bevilacqua, "Spacecraft Planar Re-phasing Guidance and Control using Input Shaping and Differential Drag", in final preparation for *AIAA Journal of Guidance, Control, and Navigation*.
- ¹³ C. E. Shannon, "Communication in the presence of noise", *Proc. Institute of Radio Engineers*, vol. 37, no. 1, pp. 10–21, Jan. 1949. Reprint as classic paper in: *Proc. IEEE*, vol. 86, no. 2, (Feb. 1998)
- ¹⁴ Perez, D., Bevilacqua, R., "Differential Drag Spacecraft Rendezvous using an Adaptive Lyapunov Control Strategy", *Acta Astronautica* 83 (2013) 196–207 <http://dx.doi.org/10.1016/j.actaastro.2012.09.005>.